J. Biomechanics Vol. 22, No. 6/7, pp. 517 521, 1989.
Printed in Great Britain

0021-9290/89 $3.00+.00
Pergamon Press plc

A DISCRETE MODEL FOR STREAMING POTENTIALS IN A SINGLE OSTEON

N. PETROV*, S. POLLACK† and R. BLAGOEVA*

*Institute of Mechanics and Biomechanics, Bulgarian Academy of Sciences, Sofia, Bulgaria;
†Department of Bioengineering, University of Pennsylvania, Philadelphia, PA, U.S.A.

Abstract—A mathematical model for streaming potentials in an osteon is proposed, taking into account the microstresses in the vicinity of the Haversian Canal. With the help of the finite element method, a boundary problem for the fluid pressure amplitude in the osteon is investigated when the bone sample is subjected to harmonic loading. A numerical analysis of the intra-osteonal potential is performed. It is found that there exists an azimuthal asymmetry which increases with the enlargement of the Haversian Canal. The results of the numerical modeling of the intra-osteonal potential are in accordance with the available experimental data.

INTRODUCTION

It is well known that bone possesses electromechanical properties which may have an important biological function in stress related bone remodeling. In a set of recent articles (Johnson *et al.*, 1980; Johnson *et al.*, 1982; Gross *et al.*, 1982; Pienkowski *et al.*, 1983; Pollack *et al.*, 1984; Anderson *et al.*, 1970; Iannacone *et al.*, 1979) two independent physical mechanisms responsible for the electromechanical behavior of bone, have been proposed—piezoelectricity and electrokinetics. The first is connected with the stress-generated electric charge separation in the bone matrix while the second one involves streaming potentials induced by the consolidation of the bone matrix during deformation. The authors have concluded that both mechanisms are operative, however, in physiologically wet bone streaming potentials quantitatively dominate.

The microelectrode studies of stress generated potentials (SGP) (Pienkowski *et al.*, 1983; Iannacone *et al.*, 1979; Starkebaum *et al.*, 1979; Pollack *et al.*, 1979) gave the opportunity to consider these potentials as a function of the bone morphology. The intra-osteonal potentials which have been obtained are characterized by large nonhomogeneity, approximate azimuthal symmetry and 'cusp-like' shapes (decreasing potential approaching the Haversian Canal on the compression side and increasing on the tension side of a bent bone specimen) due to the influence of the Haversian Canals and the cement lines of the osteons.

Recently, a model was developed for streaming potentials in the osteons (Pollack *et al.*, 1984) based on reasonable structural considerations and on first principles of electrokinetic theory and continuum mechanics. Many of the experimental results obtained by different authors for micro- and macropotentials in physiologically wet bone were explained with this model for the first time. In this way the suggestion that an electrokinetic effect was the origin of the observed SGP's was confirmed. The principal limitation of that model was that the microstress concentration around the Haversian Canal was ignored. According to Pollack *et al.*, (1979) 'the SGP's may be larger in amplitude at the Haversian Canal because of the stress concentration that occurs at the Haversian Canal' and the radial symmetry of these potentials 'can not be explained on the basis of a macrostress analysis, since the stress concentrators around an isolated hole would not result in such apparent symmetry'.

The aim of the present paper is to investigate the contribution of the microstresses on the azimuthal distribution of the streaming potentials in the osteon. Using the finite element method, the distribution of the intra-osteonal potential has been computed numerically at different values of the anatomical parameters and at various frequencies of sinusoidal loading.

PHYSICAL MODEL

Because of the complex anatomic structure of the bone it is reasonable to make the following simplifying assumptions:

1. The Haversian Canal of the osteon is considered as a cylindrical hole in a continuous isotropic medium.
2. The fluid pressure influence on the equilibrium deformation state of the matrix is taken to be small as the concentration of the fluid in compact bone is of order of 10%.
3. The fluid flux at the cement line of the osteon is taken to be equal to zero. That is not a consequence of an impermeability of the external surface of the osteon. We have in mind that the fluid pressure, and correspondingly the streaming potential, has a local extremum at the boundary between two osteons, which is in accordance with the experimental data for the micro-SGP's (Pollack *et al.*, 1979).
4. The fluid pressure in the Haversian Canal is constant and is taken to be zero. This corresponds to

Received in final form 22 *August* 1988.

the condition that the Haversian Canals in the experimental bone sample are open to atmospheric pressure.

According to Onsager's theory for an isotropic medium the following relations are valid in the absence of a diffusion flux:

$$Q = -a_{11}\nabla P + a_{12}\nabla\phi \tag{1}$$

$$J = a_{12}\nabla P - a_{22}\nabla\phi \tag{2}$$

where the generalized fluxes Q and J are the fluid volume flow rate per unit area and the total electrical current density respectively; the generalized forces are the gradients of the fluid pressure P and the electrical potential ϕ; a_{11} is the hydraulic permeability of the material, a_{22} is the electrical conductivity of the material, a_{12} is an electrokinetic coefficient, which depends on the fluid viscosity, the Zeta potential and the dielectric permitivity of fluid.

When very high input impedance voltameters are used to measure electrical potentials during deformation induced flow, J in equation (2) can be taken as zero so that the convective term must be equal and opposite to the conductive term in equation (2) hence

$$\nabla\phi = \frac{a_{12}}{a_{22}}\nabla P. \tag{3}$$

Defining the streaming potential to be equal to zero at the Haversian Canal, integration of equation (3) gives

$$\phi = \frac{a_{12}}{a_{22}}P. \tag{4}$$

In this way the problem for the computation of the streaming potential field is reduced to one of the fluid pressure field.

MECHANO-MATHEMATICAL MODEL

According to the Biot theory of consolidation (Biot, 1941) and the above simplifying assumptions the time dependence of the fluid pressure, P, is described by the equations:

$$\frac{\partial P}{\partial t} = K_1\left(\frac{\partial^2 P}{\partial X^2} + \frac{\partial^2 P}{\partial Y^2}\right) + K_2\frac{\partial}{\partial t}I(X, Y, t) \tag{5}$$

$$P(a) = 0, \quad \left.\frac{\partial P}{\partial r}\right|_{r=R} = 0 \tag{6}$$

where K_1 and K_2 are rheological constants, X and Y are Cartesian coordinates in the plane defined by a transverse section through the osteon [the micro-SGP's are measured (Starkebaum *et al.*, 1979) across the transverse sections of the osteons from sections cut transverse to the long axis of the femur of cows], $I(X, Y, t)$ is the trace of the stress tensor, a and R are radii of the Haversian Canal and the cement line of the circular cross-sectioned osteon respectively, and r is the radial coordinate in the coordinate system located at the center of the Haversian Canal.

In the microelectrode studies two deformation modes were considered—dynamic four-point bending and cyclic uniform compression. In the first mode of loading, the stress distribution across the sample can be considered linear with one half of the specimen in a state of compression, the other half in a state of tension. As the dimensions of the osteons are much smaller than the sample, the stress amplitude in pure bending in the region of a single osteon does not differ significantly across the osteon. As a result, the stress state in pure bending can be taken as the same as that induced by macroscopic homogeneous deformation. That is why in both modes the stress state in the vicinity of the Haversian Canal can be approximated with the stress field which arises around the cylindrical hole in a homogeneous medium, subjected to uniaxial loading at infinity. In this case the trace of the stress tensor is given by the sum of the radial and azimuthal stress (Timoshenko *et al.*, 1970) expressed in Cartesian coordinates as

$$I(X, Y, t) = s(t)\left[1 - 2a^2\frac{X^2 - Y^2}{(X^2 + Y^2)^2}\right] \tag{7}$$

where $s(t) = s_0\, e^{i\omega t}$ is the applied time-dependent stress at infinity, directed along the X-axis.

From equations (5), (6) and (7) the following dimensionless boundary problem for the complex amplitude of the fluid pressure is obtained:

$$\frac{\partial^2\tilde{P}}{\partial\bar{X}^2} + \frac{\partial^2\tilde{P}}{\partial\bar{Y}^2} - i\bar{w}\tilde{P} + i\bar{w}I(\bar{X}, \bar{Y}) = 0 \tag{8}$$

$$\tilde{P}(a) = 0, \quad \left.\frac{\partial\tilde{P}}{\partial\bar{r}}\right|_{\bar{r}=1} = 0 \tag{9}$$

where $\tilde{P}$ is the complex amplitude of the pressure defined by the expression

$$P = K_2 s_0 \tilde{P}\, e^{iwt}$$

and

$$\bar{X} = \frac{X}{R}, \quad \bar{Y} = \frac{Y}{R}, \quad \bar{r} = \frac{r}{R}, \quad \bar{w} = \frac{R^2}{K_1}w$$

and

$$I(\bar{X}, \bar{Y}) = \left[1 - \frac{2a^2}{R^2}\frac{\bar{X}^2 - \bar{Y}^2}{(\bar{X}^2 + \bar{Y}^2)^2}\right].$$

Having in mind equation (4), the results for the dimensionless amplitude of the fluid pressure can be directly used for the evaluation of the intra-osteonal potential.

Equations (8) and (9) can be transformed into a system of linear algebraic equations using the Galercan method of finite elements. By symmetry it is necessary to solve the problem in only one quadrant and Fig. 1 shows the mesh used to evaluate $\tilde{P}$ at each node. Discretization of the problem is achieved by defining a system of nodes at X^K, where X^K is the

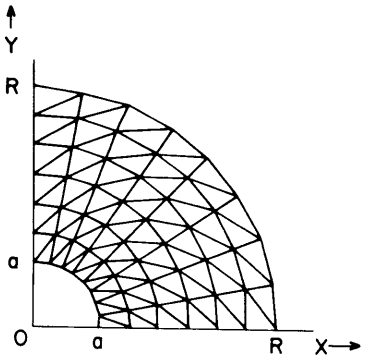

Fig. 1. Finite element grid shown for one quadrant of an osteon where a is the radius of the Haversian Canal.

position of the Kth node, and interpolation functions $v^K(X)$ where

$$v^K(X^L)=\begin{cases} 1; & K=L \\ 0; & K\neq L \end{cases} \tag{10}$$

Approximating $\tilde{P}$ as $\hat{P}$, where

$$\hat{P}\equiv\sum_{K=1}^{N}\tilde{P}^K v^K(X) \tag{11}$$

and where $\tilde{P}^K$ are the values of $\tilde{P}$ at X^K then equation (8) becomes

$$\left(\frac{\partial^2}{\partial\bar{X}^2}+\frac{\partial^2}{\partial\bar{Y}^2}-i\bar{w}\right)\hat{P}+i\bar{w}I(\bar{X},\bar{Y})=\varepsilon \tag{12}$$

where ε is the error resulting from the approximation introduced in equation (11). Multiplying equation (12) by $v^K(X)$, replacing $\hat{P}$ by equation (11), and using appropriate vector identities gives

$$-\sum_{L=1}^{N}(\nabla v^L(X)\cdot\nabla v^K(X)\,\tilde{P}^L-i\bar{w}\sum_{L=1}^{N}(v^K(X)v^L(X))\tilde{P}^L$$
$$+i\bar{w}I(\bar{X},\bar{Y})v^K(X)+\sum_{L=1}^{N}\nabla\cdot(v^K(X)\nabla v^L(X))\,\tilde{P}^L$$
$$=\varepsilon v^K(X). \tag{13}$$

Integrating over the volume V, and using the Galercan condition that

$$\int_V \varepsilon v^K(X)\,\mathrm{d}V=0 \tag{14}$$

gives

$$\sum_{L=1}^{N}(S_{KL}+i\bar{w}C_{KL})\tilde{P}^L=R^K+F^K \tag{15}$$

where

$$S_{KL}=\int_V \nabla v^L(X)\cdot\nabla v^K(X)\,\mathrm{d}V \tag{16}$$

$$C_{KL}=\int_V v^K(X)v^L(X)\,\mathrm{d}V \tag{17}$$

$$R_K=i\bar{w}\int_V I(\bar{X},\bar{Y})v^K(X)\,\mathrm{d}V \tag{18}$$

$$F_K=\sum_{L=1}^{N}\int_V \nabla\cdot(v^K(X)\nabla v^L(X))\,\tilde{P}^L\,\mathrm{d}V \tag{19}$$

$$F_K=\sum_{L=1}^{N}\int_S v^K(X)(\nabla v^L(X))_{\text{Normal}}\,\tilde{P}^L\,\mathrm{d}S. \tag{20}$$

The surface integral in equation (20) is obtained from equation (19) by the divergence theorem and, using equation (11), can be rewritten as

$$F_K=\int_S v^K(X)(\nabla\hat{P})_{\text{Normal}}\,\mathrm{d}S \tag{21}$$

and is evaluated by the boundary conditions at a and R (equation 6) such that $F_K=0$.

Equation 14 is evaluated for each $\tilde{P}^L$, the absolute magnitude being the amplitude of the fluid pressure at each node L and the phase being the phase relative to the applied stress. From equation (4), the solution to the pressure gives the solution to the stress-generated potential.

RESULTS AND CONCLUSIONS

Figures 2 and 3 show equipotential lines of the peak (real) amplitude normalized by the maximum value for a typical osteon whose ratio of the Haversian Canal radius to the radius of the cement line (a/R) is equal to 0.27. The applied stress is taken as sinusoidal with a dimensionless frequency $\bar{w}=0.01$ in Fig. 2 and $\bar{w}=0.1$ in Fig. 3.

The azimuthal asymmetry caused by the stress concentration around the Haversian Canal can be

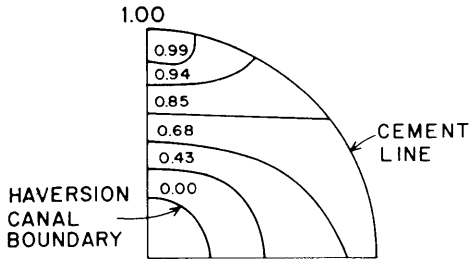

Fig. 2. Equipotential lines of normalized peak potential in an osteon with $a/R=0.27$ and $\bar{w}=0.01$.

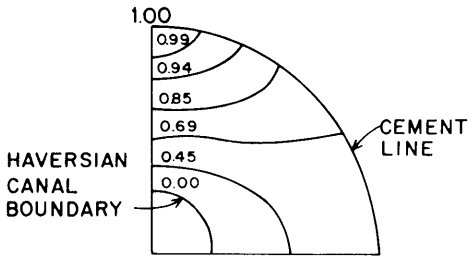

Fig. 3. Equipotential lines of normalized peak potential in an osteon with $a/R=0.27$ and $\bar{w}=0.1$.

characterized by defining the parameter $\tilde{\phi}$, where

$$\tilde{\phi} = \frac{\phi^y_{max} - \phi^x_{max}}{\phi^y_{max}} \quad (21)$$

and where ϕ^y_{max} is the maximum value of the normalized peak potential in the y direction (this occurs at the cement line) and ϕ^x_{max} is the same in the x direction. Figure 4 shows $\tilde{\phi}$ as a function of a/R. The dashed portion of the curve is an extrapolation to $\tilde{\phi}=0$ at $a/R=0$. For typical osteons for which a/R is between 0.2 and 0.3, $\tilde{\phi}$ is approximately equal to 0.3 and reaches a value of 0.42 when $a/R=0.5$. It is interesting to note that values of a/R greater than 0.5 can be found in osteons in severe osteoporotic cases and in such cases this asymmetry is quite large.

The radial dependence of the potential from the Haversian Canal to the cement line has been described (Starkebaum *et al.*, 1979) as cusp-like. This is computed along the y axis for $\bar{w}=0.01$ and is plotted in Fig. 5. ϕ^y is normalized by ϕ^y_{max} and the y coordinate is normalized as shown. The solid curve shows the results obtained here and the data points are taken

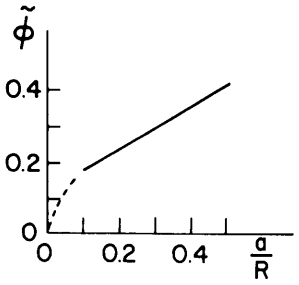

Fig. 4. Normalized azimuthal asymmetry in the maximum value of the potential as a function of the ratio of the Haversian Canal radius to the radius of the cement line (a/R)

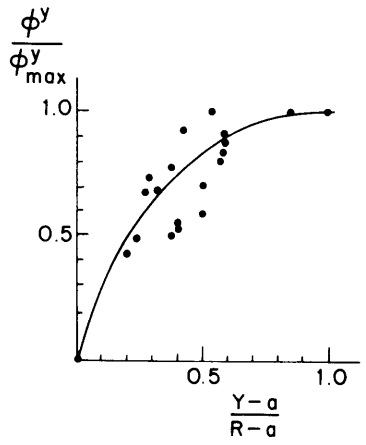

Fig. 5. The radial dependence of the potential along the y-axis (ϕ^Y) normalized by the maximum value of the potential (ϕ^Y_{max}) at the cement line vs the normalized y-coordinate. Solid curve is the result of the numerical method used here. The points are data from the literature (Iannacone *et al.*, 1979; Starkebaum *et al.*, 1979).

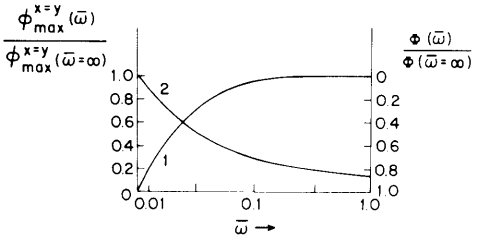

Fig. 6. The potential at the cement line at $x=y$ ($\phi^{x=y}_{max}(\bar{\omega})$) normalized by the same potential at $\bar{w} \rightarrow \infty$, ($\phi^{x=y}_{max}(w=\infty)$) plotted as a function of $\bar{w}$. The phase Φ of $\phi^{x=y}_{max}(\bar{w})$ normalized by the phase of $\phi^{x=y}_{max}(\bar{w}=\infty)$ is also shown as a function of $\bar{w}$.

from the literature (Iannacone *et al.*, 1979; Starkebaum *et al.*, 1979). Reasonable agreement is obtained indicating that the cusp-like potentials are also predicted by this numerical approximation.

The microstresses within the osteon are equal to the macrostresses only along the direction $x=y$ according to equation (7). The maximum value of the potential $\phi^{x=y}_{max}$ along this axis (i.e the value of the potential at the cement line) and the phase are shown in Fig. 6 as a function of the dimensionless frequency $\bar{w}$. $\phi^{x=y}_{max}$ is normalized by the value of $\phi^{x=y}_{max}$ when $\bar{w} \rightarrow \infty$. The functional form of the curves in Fig. 6 are the same as those derived by Salzstein *et al.* (1987) for the amplitude and phase of the macropotentials for a bent beam of bone. This suggests that the same physical mechanism is responsible for the micropotentials in bone as for the macropotentials as originally proposed by Pienkowski *et al.* (1983).

Acknowledgements—The authors wish to thank the National Science Foundation (Grants ECS 84-11335 and INF 81-08481) and the Bulgarian Academy of Sciences for their continued support throughout this collaborative study.

REFERENCES

Anderson, J. C. and Eriksson, C. (1970) Piezoelectric properties of dry and wet bone. *Nature* **2227**, 491–492.

Biot, M. (1941) General theory of three-dimensional consolidation. *J. appl. Phys.* **12**, 155–164.

Gross, D. and Williams, W. S. (1982) Streaming potential and the electromechanical response of physiologically moist bone. *J. Biomechanics* **15**, 277–292.

Iannacone, W., Korostoff, E. and Pollack, S. R. (1979) Microelectrode studies of SGP obtained from uniform and nonuniform compression of human bone. *JBMR* **13**, 753–763.

Johnson, M. W., Chakkalakal, D. A., Harper, R. A. and Katz, J. L. (1980) Comparison of the electromechanical effects in wet and dry bone. *J. Biomechanics* **13**, 437–442.

Johnson, M. W., Chakkalakal, D. A., Harper, R. A., Katz, J. L. and Rauhanan, S. W. (1982) Fluid flow in bone *in vitro*. *J. Biomechanics* **15**, 881–885.

Pienkowski, D. and Pollack, S. R. (1983) The origin of stress potentials in fluid saturated bone. *J. Orthop. Res.* **1**, 30–41.

Pollack, S. R., Korostoff, E., Starkebaum, W. and Iannacone, W. (1981) Microelectrode studies of stress generated potentials in bone. *Electrical Properties of Bone and Cartilage.* (edited by Brighton, C. T. Black, J. and Pollack, S. R.) Grune & Stratton, NY.

Pollack, S. R., Salzstein, R. and Pienkowski, D. (1984) Streaming potentials in fluid filled bone. *Ferroelectrics* **60,** 297–309.

Pollack, S. R., Petrov, N., Salzstein, R., Brankov, G. and Blagoeva, R. (1984) An anatomical model for streaming potentials in osteons. *J. Biomechanics* **17,** 627–636.

Salzstein, R, Pollack, S. R., Mak, A. and Petrov, N. (1987) Electromechanical potentials in cortical bone—I. A continuum approach. *J. Biomechanics* **20,** 261–270.

Starkebaum, W. S., Pollack, S. R. and Korostoff, E. (1979) Microelectrode studies of stress-generated potentials in four-point bending of bone. *J. Biomed. Mat. Res.* **13,** 729–751.

Timoshenko, S. P. and Goodier, J. N. (1970) *Theory of Elasticity*. p. 61, McGraw-Hill, NY.